

# Electrical detection of single viruses

Fernando Patolsky<sup>\*†</sup>, Gengfeng Zheng<sup>\*†</sup>, Oliver Hayden<sup>\*</sup>, Melike Lakadamyali<sup>‡</sup>, Xiaowei Zhuang<sup>\*\*§</sup>, and Charles M. Lieber<sup>\*§¶</sup>

Departments of <sup>\*</sup>Chemistry and Chemical Biology and <sup>†</sup>Physics and <sup>¶</sup>Division of Engineering and Applied Sciences, Harvard University, Cambridge, MA 02138

Contributed by Charles M. Lieber, August 20, 2004

**We report direct, real-time electrical detection of single virus particles with high selectivity by using nanowire field effect transistors. Measurements made with nanowire arrays modified with antibodies for influenza A showed discrete conductance changes characteristic of binding and unbinding in the presence of influenza A but not paramyxovirus or adenovirus. Simultaneous electrical and optical measurements using fluorescently labeled influenza A were used to demonstrate conclusively that the conductance changes correspond to binding/unbinding of single viruses at the surface of nanowire devices. pH-dependent studies further show that the detection mechanism is caused by a field effect, and that the nanowire devices can be used to determine rapidly isoelectric points and variations in receptor-virus binding kinetics for different conditions. Lastly, studies of nanowire devices modified with antibodies specific for either influenza or adenovirus show that multiple viruses can be selectively detected in parallel. The possibility of large-scale integration of these nanowire devices suggests potential for simultaneous detection of a large number of distinct viral threats at the single virus level.**

Viruses are among the most important causes of human disease (1–3) and an increasing concern as agents for biological warfare and terrorism (4, 5). Rapid, selective, and sensitive detection of viruses is central to implementing an effective response to viral infection, such as through medication or quarantine. Established methods for viral analysis include plaque assays, immunological assays, transmission electron microscopy, and PCR-based testing of viral nucleic acids (2, 6, 7). These methods have not achieved rapid detection at a single virus level and often require a relatively high level of sample manipulation that is inconvenient for infectious materials. Yet, the ability to detect rapidly, directly, and selectively individual virus particles has the potential to significantly impact health care, since it could enable diagnosis at the earliest stages of replication within a host's system.

One promising approach for the direct electrical detection of biological macromolecules uses semiconducting nanowires or carbon nanotubes configured as field-effect transistors, which change conductance upon binding of charged macromolecules to receptors linked to the device surfaces (8–11). Previous studies have reported conductance changes caused by selective binding of large numbers of a specific protein or nucleic acid sequence at a device surface by using purified samples. However, this work does not indicate that selective detection at a single particle level (that is, stochastic sensing) is possible with nanowire or nanotube field-effect transistors. In addition to meeting this challenge of single particle detection with these nanoscale devices, stochastic sensing offers important scientific advantages, including the following: selective detection is not limited by the affinity of the receptor as in previous equilibrium measurements; analysis of single particle on/off times provides direct information about binding kinetics crucial to understanding, for example, virus-receptor interactions (12, 13); and single particle sensitivity could enable simple charge-based detection of macromolecules.

## Materials and Methods

**Nanowire Device Arrays.** Silicon nanowires were synthesized by chemical vapor deposition with 20-nm gold nanoclusters as

catalysts, silane as reactant, and diborane as p-type dopant with a B/Si ratio of 1:4,000. Arrays of silicon nanowire devices were defined by using photolithography with Ni metal contacts (14) on silicon substrates with a 600-nm-thick oxide layer. The metal contacts to the nanowires were isolated by subsequent deposition of  $\approx 50$ -nm-thick  $\text{Si}_3\text{N}_4$  coating. The spacing between source-drain electrodes (active sensor area) was 2  $\mu\text{m}$  in all experiments.

Virus samples were delivered to the nanowire device arrays by using fluidic channels formed by either a flexible polymer channel (8) or a 0.1-mm-thick glass coverslip sealed to the device chip. Virus samples were delivered through inlet/outlet connection in the polymer or holes made through the back of device chip in the case of the coverslip. Similar electrical results were obtained with both approaches, although the latter was used for all combined electrical/optical measurements.

**Nanowire Surface Modification.** A two-step procedure was used to covalently link antibody receptors to the surfaces of the silicon nanowire devices. First, the devices were reacted with a 1% ethanol solution of 3-(trimethoxysilyl)propyl aldehyde (United Chemical Technologies, Bristol, PA) for 30 min, washed with ethanol, and heated at 120°C for 15 min. Second, mAb receptors, anti-hemagglutinin for influenza A (AbCam, Cambridge, U.K.) and anti-adenovirus group III (Charles River Breeding Laboratories), were coupled to the aldehyde-terminated nanowire surfaces by reaction of 10–100  $\mu\text{g}/\text{ml}$  antibody in a pH 8, 10-mM phosphate buffer solution containing 4 mM sodium cyanoborohydride. The surface density of antibody was controlled by varying the reaction time from 10 min (low density) to 3 h (high density). Unreacted aldehyde surface groups were subsequently passivated by reaction with ethanolamine under similar conditions. Device arrays for multiplexed experiments were made in the same way except that distinct antibody solutions were spotted on different regions of the array. The antibody surface density vs. reaction time was quantified by reacting Au-labeled IgG antibodies (Ted Pella, Inc., Redding, CA; 5-nm Au nanoparticles) with aldehyde-terminated nanowires on a transmission electron microscopy grid, and then imaging the modified nanowire by transmission electron microscopy, which enabled the number of antibodies per unit length of nanowire to be counted (Fig. 6, which is published as supporting information on the PNAS web site).

**Virus Samples.** Different concentration virus solutions were prepared from stocks by dilution in phosphate buffer (10  $\mu\text{M}$ , pH 6.0) containing 10  $\mu\text{M}$  KCl (assay buffer); influenza type A,  $10^9$  to  $10^{10}$  particles per ml [Charles River Breeding Laboratories; purified virus supplied in 0.1 M Hepes buffer (pH 7.4), caprolactane inactivated], and unpurified avian adenovirus group III, influenza A, and avian paramyxovirus virus in allantoic fluid,  $10^{10}$  to  $10^{11}$  particles per ml (Charles River Breeding Labora-

Freely available online through the PNAS open access option.

<sup>†</sup>F.P. and G.Z. contributed equally to this work.

<sup>§</sup>To whom correspondence may be addressed. E-mail: zhuang@chemistry.harvard.edu or cml@cmliris.harvard.edu.

© 2004 by The National Academy of Sciences of the USA

tories), were used as received after dilution in assay buffer or purified by using a microfiltration device (5,000 rpm, Centricon 30, Millipore). Similar results (sensitivity and selectivity) were obtained with purified and unpurified samples. Viral concentrations were measured by transmission electron microscopy after staining samples with uranyl acetate and by fluorescence microscopy using 1,1'-dioctadecyl-3,3,3',3'-tetramethylindocarbocyanine-labeled viruses.

**Electrical Measurements.** Electrical measurements were made by using lock-in detection with a modulation frequency chosen as a prime number between 17 and 79 Hz, inclusive. Measurements were independent of frequency within this range. The modulation amplitude was 30 mV and the dc source-drain potential was zero to avoid electrochemical reactions. Conductance vs. time data were recorded while buffer solutions, or different virus solutions, flowed through the microfluidic channel. Viral sensing experiments were performed in the microfluidic channel under a flow rate of 0.15 ml/hr in 10  $\mu$ M phosphate buffer solution containing 10  $\mu$ M KCl at pH 6.0.

**Optical Imaging.** Influenza virus solutions containing  $10^8$  virus particles per ml were labeled with DiIC<sub>18</sub> (Molecular Probes) in a manner similar to previous studies (15). Optical data were acquired by using a Zeiss LSM 510 laser scanning confocal microscope with PMT detectors and water immersion objective ( $\times 60$ , numerical aperture 1.2). The DiIC<sub>18</sub> dye was excited at 532 nm. Bright-field and fluorescence images together with conductance data were recorded simultaneously. The bright-field data, which highlight the positions of the nanowire and passivated metal contact electrodes, and fluorescence data were recorded simultaneously with two detectors and combined to show the relative positions of the nanowire and moving virus particles.

## Results and Discussion

The underlying concept of our experiments is illustrated schematically in Fig. 1: when a virus particle binds to the antibody receptor on a nanowire device, the conductance of that device should change from the baseline value, and when the virus unbinds, the conductance should return to the baseline value. For a p-type nanowire, the conductance should decrease (increase) when the surface charge of the virus is positive (negative) (8). The conductance of a second nanowire device at which binding does not occur during this same time period should show no change and can serve as an internal control. Modification of different nanowires within the array with receptors specific for different viruses provides a means for simultaneous detection of multiple viruses.

We have used arrays of individually addressable silicon nanowire field-effect transistors, which exhibit reproducible high-performance properties (14, 16), for these experiments. Representative microscopy images of a silicon nanowire device array are shown in Fig. 2. The nanowire elements were confined to a central region that was coupled to a microfluidic channel for sample delivery; the larger-scale metal electrodes, which are used for electrical connections to measurement instrumentation, were passivated with silicon nitride in all areas exposed to solution. Nanowire elements within the arrays were functionalized with the same or different virus-specific antibodies as receptors for selective binding.

Time-dependent conductance data recorded simultaneously from two nanowires in the same device array modified with antibodies specific for influenza A virus (Fig. 3A) show discrete changes in conductance when a solution containing  $\approx 100$  virus particles per  $\mu$ l is delivered to the sensor elements. There are several key features of these experiments. First, the magnitude and duration of the conductance drops are nearly the same for a given nanowire: for nanowires 1 and 2 the magnitude and

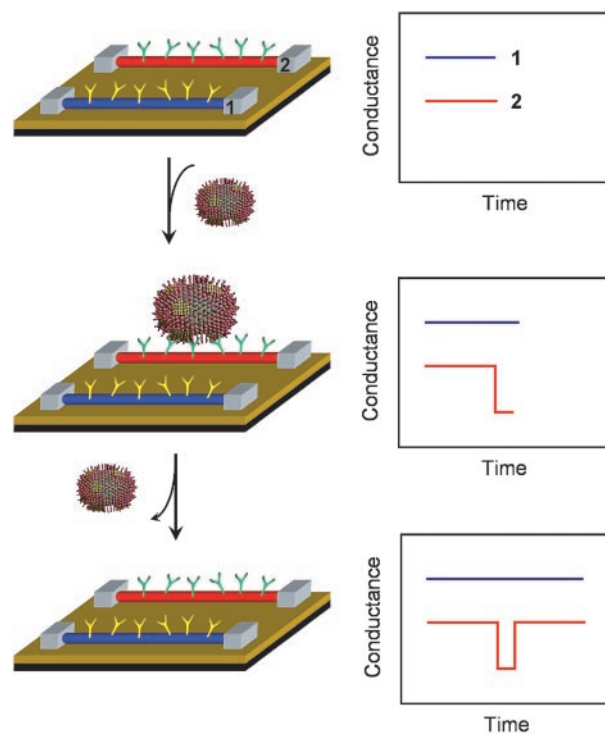


**Fig. 1.** Nanowire-based detection of single viruses. (Left) Schematic shows two nanowire devices, 1 and 2, where the nanowires are modified with different antibody receptors. Specific binding of a single virus to the receptors on nanowire 2 produces a conductance change (Right) characteristic of the surface charge of the virus only in nanowire 2. When the virus unbinds from the surface the conductance returns to the baseline value.

duration are  $24 \pm 1$  nS and  $20 \pm 4$  s, and  $20 \pm 3$  nS and  $15 \pm 7$  s, respectively. The similarity in responses is consistent with good reproducibility in the nanowires electronic properties (14) and a uniform density of antibody receptors on their surfaces, which determine the response to and duration of binding of a single virus, respectively. Second, an excess of free antibody added to the viral solution (monoclonal anti-hemagglutinin for influenza A was added to a standard solution containing 100 virions per  $\mu$ l to yield an antibody concentration of 10  $\mu$ g/ml) eliminates the well defined conductance changes consistent with blocking sites on the viruses that are recognized by the same antibodies attached to the nanowire surfaces. Lower antibody concentrations produced partial reduction of the nanowire response. Third, the discrete conductance changes are uncorrelated for the two nanowire devices in the microfluidic channel and are thus consistent with stochastic binding events at or near the surfaces of the respective nanowires. Fourth, concentration-dependent measurements show that the frequency of the discrete conductance drops is directly proportional to the number of virus particles in solution (Fig. 3A Inset and Fig. 7, which is published as supporting information on the PNAS web site). The observed frequencies also agree with estimates for a diffusion limited process (17). Lastly, little or no purification of virus samples is required in these measurements; that is, similar results were obtained on samples purified by simple gel filtration or diluted directly from allantoic fluid.

Measurements were also made as a function of pH at constant ionic strength to probe viral surface charge. These data (Fig. 3B and Fig. 8, which is published as supporting information on the PNAS web site) show that the discrete conductance changes decrease and then increase in magnitude but with opposite sign as the pH increases from 5.5 to 8 with a point of zero conduc-

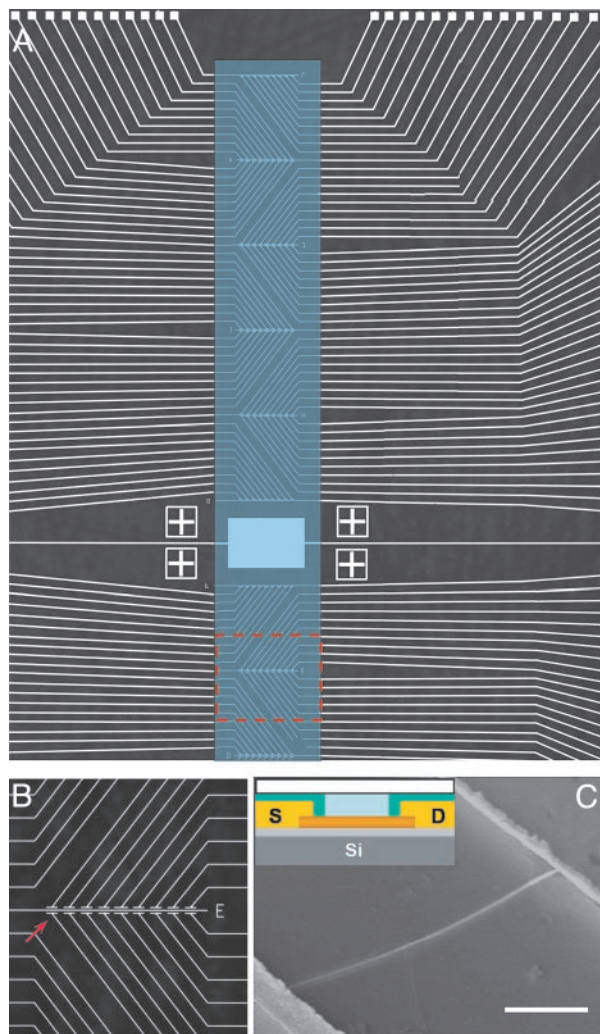


**Fig. 2.** Nanowire devices and device array. (A) Optical image of the upper portion of a device array. White lines correspond to metal electrodes that connect to individual nanowire devices. The position of the microfluidic channel used to deliver sample is highlighted in blue and has a total size of  $6 \text{ mm} \times 500 \mu\text{m}$ , length  $\times$  width. The image field is  $4.4 \times 3.5 \text{ mm}$ . (B) Optical image of one row of addressable device elements from the region highlighted by the red-dashed box in A. The red arrow highlights the position of a device. The image field is  $500 \times 400 \mu\text{m}$ . (C) Scanning electron microscopy image of one silicon nanowire device. The electrode contacts are visible at the upper right and lower left regions of the image. (Scale bar:  $500 \text{ nm}$ .) (Inset) Cross-sectional schematic of a single silicon nanowire device. The nanowire (orange horizontal line) is connected at its ends by source (S) and drain (D) metal electrodes (gold), and metal is insulated with a layer of silicon nitride (green). The microfluidic channel is indicated (blue).

tance change (that is, the isoelectric point) occurring between pH 6.5 and 7.0. The results and estimated isoelectric point are consistent with our electrophoretic mobility measurements made by using much higher concentrations and larger quantities of virus. The fact that the p-type nanowire devices show a reduced (increased) conductivity upon binding of single influenza A viruses at  $\text{pH} < 7$  ( $\geq 7$ ) also demonstrates clearly that detection with the nanowire devices is caused by a field effect and not a change in capacitance as reported for carbon nanotube sensors (11). More generally, our results suggest that these nanowire devices could be used to determine rapidly isoelectric points for small quantities of viruses and other biomolecules. In addition, the time scale of the discrete changes in conductance associated with binding/unbinding depends on pH (Fig. 8),

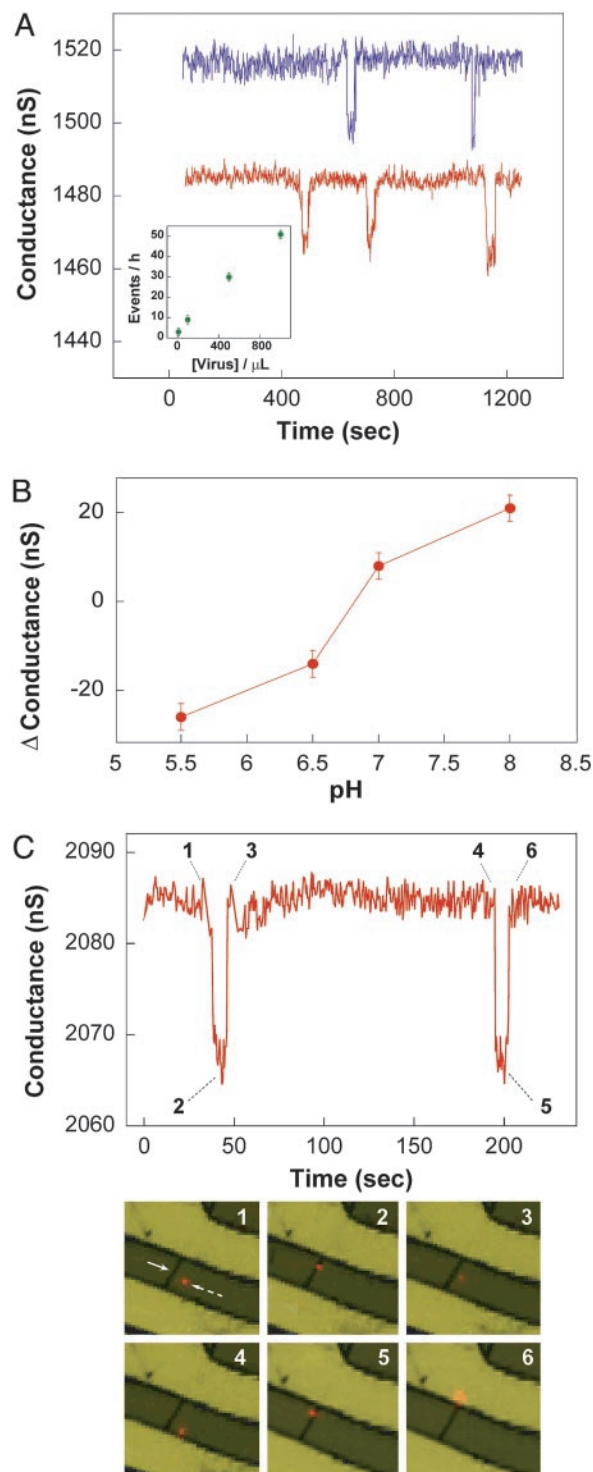


**Fig. 3.** Selective detection of single viruses. (A) Conductance vs. time data recorded simultaneously from two silicon nanowires elements, red and blue plots, within a single device array after introduction of an influenza A solution. (Inset) Frequency of single virus events as a function of virus solution concentration. (B) Conductance changes associated with single influenza A virus binding/unbinding as a function of solution pH. (C) Conductance (Upper) and optical (Lower) data recorded simultaneously vs. time for a single silicon nanowire device after introduction of influenza A solution. Combined bright-field and fluorescence images correspond to time points 1–6 indicated in the conductance data; virus appears as a red dot in the images. The solid white arrow in image 1 highlights the position of the nanowire device, and the dashed arrow indicates the position of a single virus. Images are  $8 \times 8 \mu\text{m}$ . All measurements were performed with solutions containing 100 viral particles per  $\mu\text{L}$ .

which suggests that nanowire detectors could be used to assess directly variations in receptor–virus binding kinetics (for different conditions) from the single particle binding/unbinding data (12, 13).

To characterize the discrete conductance changes further, we have carried out simultaneous electrical and optical measurements. Parallel collection of conductance, fluorescence, and bright-field data from a single nanowire device (Fig. 3C) with fluorescently labeled viruses demonstrates clearly that each discrete conductance change corresponds to a single virus binding to and unbinding from the nanowire. Although providing an independent assay of the binding/unbinding of single viruses at nanowire surfaces, it should be stressed that the optical measurements require specific labeling with fluorescent molecules and subsequent purification, which would make them difficult to implement as a sensor. The data (Movie 1, which is published as supporting information on the PNAS web site) show that as a virus particle diffuses near a nanowire device the conductance remains at the baseline value, and only after binding at the nanowire surface does the conductance drop, where the conductance change,  $18 \pm 1$  nS, is similar to that observed with unlabeled viruses; as the virus unbinds and diffuses from the nanowire surface the conductance returns rapidly to the baseline value. Movie 1 further shows that a bound virus can sample several nearby positions on the nanowire surface before unbinding, which may explain the smaller variations in conductance in the on state. The two events in Fig. 3C also exhibit similar conductance changes when virus particles bind to distinct sites on the nanowire, and thus demonstrate that the detection sensitivity is relatively uniform along the length of the nanowire. Lastly, these parallel measurements indicate that a virus particle must be in contact with the nanowire device to yield an electrical response, thus suggesting the potential for relatively dense integration without crosstalk.

Selective detection, the ability to specifically distinguish one type of virus from another, is crucial for exploiting the high sensitivity of these nanowire devices in most medical and biothreat applications. Selectivity was first investigated by characterizing how variations in the density of the influenza A antibody receptors affect the binding/unbinding properties. Simultaneous conductance and optical data recorded on devices with average antibody coverage  $\approx 10$  times higher than above (Fig. 4A and Movie 2, which is published as supporting information on the PNAS web site) show sequential binding of virus particles without unbinding on a 5- to 10-min time scale (vs. unbinding on a 20-s time scale in Fig. 3). Sequential unbinding of the viruses is observed after introducing pure buffer solution. These data show that the unbinding kinetics can be substantially slowed through increases in the density of specific antibodies and provide strong evidence for selective binding of influenza A; that is, the unbinding kinetics should be slowed as the number of specific antibody–virus contact points increases.

In addition, parallel electrical and optical experiments carried out on devices with a low density of specific antibodies (Fig. 4B) show discrete conductance changes caused by the interaction of single viruses with an average duration,  $1.1 \pm 0.3$  s. This average on time is  $\approx 20$  times shorter than observed in Fig. 3, where an intermediate antibody density was used. Careful analysis shows that some of the conductance changes (e.g., event 2) have a time scale of 1–1.5 s, although other events have a time scale of  $0.4 \pm 0.1$  s that is characteristic of diffusion of the virus past and/or rapid touching of the nanowire surface (see below). Interestingly, further analysis of event 2 (Movie 3, which is published as supporting information on the PNAS web site) shows that the virus rapidly samples two nearby positions on the nanowire surface before unbinding. Overall, these coverage-dependent detection data are consistent with selective detection and the ability to vary unbinding kinetics with the density of specific

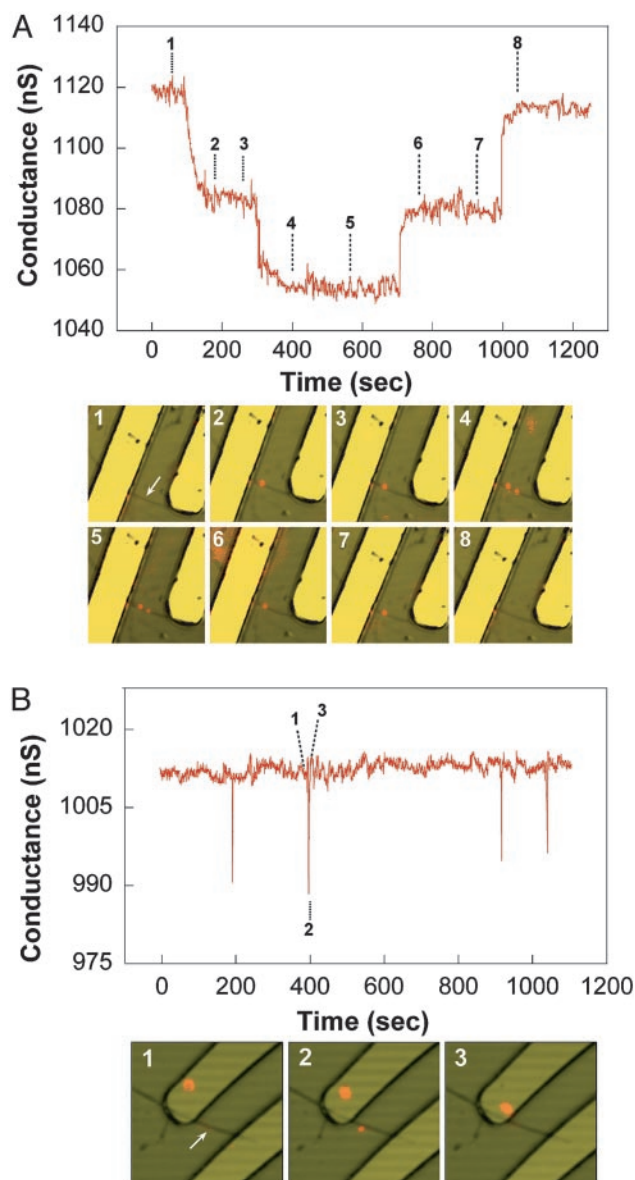


**Fig. 4.** Single virus binding selectivity. (A) Simultaneous conductance and optical vs. time data recorded from a single nanowire device with a high density of anti-influenza type A antibody. Influenza A solution was added before point 1, and the solution was switched to pure buffer between points 4 and 5 on the plot. The bright-field and fluorescence images corresponding to time points 1–8 are indicated in the conductance data; the viruses appear as red dots in the images. Each image is  $6.5 \times 6.5 \mu\text{m}$ . (B) Simultaneous conductance and optical vs. time data recorded from a single nanowire device with a low density of anti-influenza type A antibody. Bright-field and fluorescence images corresponding to time points 1–3 are shown. Each image is  $7 \times 7 \mu\text{m}$ . Measurements were made by using solutions containing 100 viral particles per  $\mu\text{l}$ . The solid white arrows highlight the positions of the nanowires in both devices.

antibodies. These experiments further suggest that it should be possible in the future to determine the unbinding kinetics from a single antibody or other receptor, and how the interactions are perturbed, for example, by the addition of small molecules.

Critical to the potential development of detection devices is selectivity for different viral threats. Delivery of a solution containing influenza A (100 virions per  $\mu\text{l}$ ) to a nanowire device functionalized with a high density of anti-adenovirus group III antibodies, which should have no specificity against influenza A,

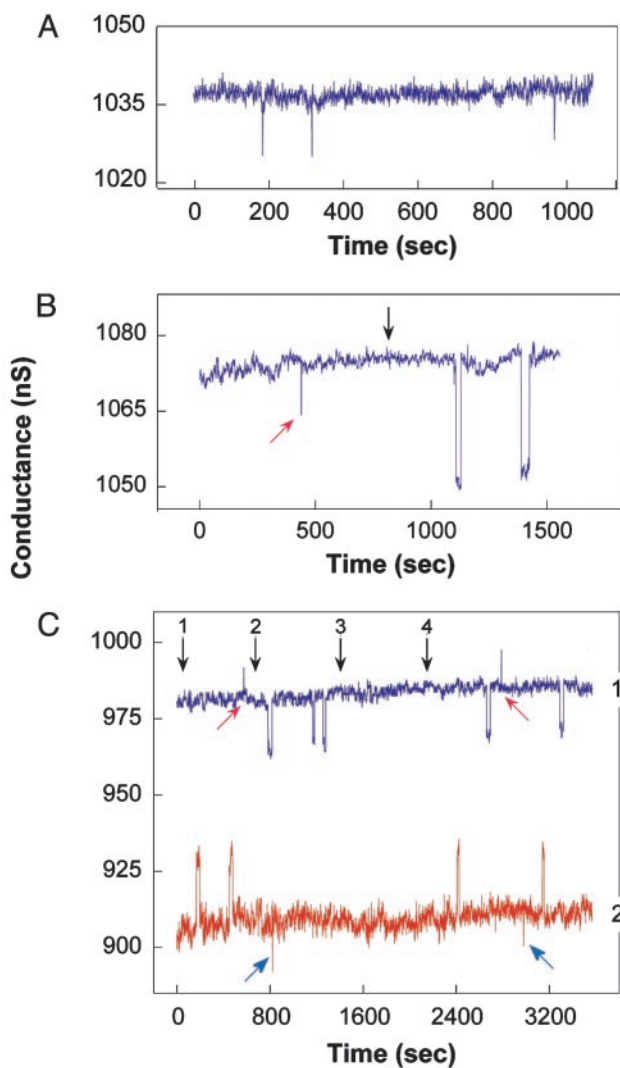


**Fig. 5.** Selective and multiplexed single virus detection. (A) Conductance vs. time curve recorded from a silicon nanowire device after introduction of influenza A virus solution; the device had a high surface coverage of anti-adenovirus group III antibody. (B) Conductance vs. time data recorded from a silicon nanowire device modified with an intermediate density of anti-influenza type A antibody. Initially, a solution of paramyxovirus (50 virions per  $\mu\text{l}$ ) was delivered to the device, and at the point indicated by black arrow the solution was changed to one containing influenza A (50 virions per  $\mu\text{l}$ ). (C) Conductance vs. time data recorded simultaneously from two silicon nanowires elements; one nanowire (nanowire 1) was modified with anti-influenza type A antibody (blue data), and the other (nanowire 2) was modified with anti-adenovirus group III antibody (red data). Black arrows 1–4 correspond to the introduction of adenovirus, influenza A, pure buffer, and a 1:1 mixture of adenovirus and influenza A, where the virus concentrations were 50 viral particles per  $\mu\text{l}$  in phosphate buffer (10  $\mu\text{M}$ , pH 6.0). Small red and blue arrows in B and C highlight conductance changes corresponding to diffusion of viral particles past the nanowire and not specific binding.

only exhibited discrete conductance changes of short duration,  $0.4 \pm 0.1$  s (Fig. 5A). These short events are consistent with diffusion of the virus past and/or rapid touching of the nanowire surface and can be readily distinguished on the basis of temporal behavior from selective binding exhibited by devices with a comparable density of specific antibody (Fig. 4A). A more stringent test of selectivity was also carried out by characterizing the response of a device to two different, but structurally similar, viruses, paramyxovirus and influenza A, by using nanowire devices modified with antibodies specific for influenza A (Fig.

5B). Delivery of a solution containing paramyxovirus exhibited only short-duration conductance changes characteristic of diffusion of the virus past and/or rapid touching of the nanowire surface and not specific binding; however, when the solution was changed to one containing influenza A, conductance changes consistent with well defined binding/unbinding behavior similar to that in Fig. 3 were observed. Importantly, these experiments demonstrate that the antibody-modified nanowire devices exhibit excellent binding selectivity, which is an important characteristic for detection of one or more viruses. Although not our focus, these data also show that the devices are sensitive to single charged virus particles (including the sign of the charge) as they diffuse by and sample the nanowire surface, and this capability could find uses, for example, for charge detection in microfluidic devices.

Lastly, we investigated multiplexed detection of different viruses at the single particle level by modifying nanowire device surfaces in an array with antibody receptors specific either for influenza A (nanowire 1) or adenovirus (nanowire 2). Simultaneous conductance measurements obtained when adenovirus, influenza A, and a mixture of both viruses are delivered to the devices (Fig. 5C) show several key points. Introduction of adenovirus, which is negatively charged at the pH of the experiment (18), to the device array yields positive conductance changes for nanowire 2 with an on time of  $16 \pm 6$  s, similar to the selective binding/unbinding in Fig. 3 for a comparable density of surface receptors. The magnitude of the conductance change for binding of single adenovirus particles differs from that of influenza A viruses because of differences in the surface charge densities for the two viruses. Shorter,  $\approx 0.4$ -s duration positive conductance changes are also observed for nanowire 1. These changes are characteristic of a charged virus diffusing past and rapidly sampling the nanowire element (see above) and can be readily distinguished from specific binding to the antibody receptors. On the other hand, addition of influenza A yields negative conductance changes for nanowire 1, with a binding/unbinding behavior similar to that in Fig. 3 under comparable conditions. Nanowire 2 also exhibits short duration negative conductance changes, which likely correspond to diffusion of influenza A viral particles past the nanowire device, although these are also readily distinguished from specific binding events by the temporal response. Significantly, delivery of a mixture of both viruses demonstrates unambiguously that selective binding/unbinding responses for influenza A and adenovirus can be detected in parallel by nanowire 1 and nanowire 2, respectively, at the single virus level.

Our studies show that single viruses can be detected directly with high selectivity, including parallel detection of different viruses, in electrical measurements using antibody functionalized nanowire field-effect transistors. This demonstrated potential, which was achieved with virtually unpurified samples, could impact virus detection for medical and biothreat applications and exceeds the capabilities of existing methods such as PCR (2, 7, 19) and micromechanical devices (20). PCR-based detection approaches can be used to identify a number of virus types, but cannot be carried out reliably at the single virus level and are intrinsically much slower (because of multiple reaction and purification steps) than our direct method (2, 19). Recent studies of micro/nanomechanical devices (20) have reported the capability of detecting the mass change associated with binding of a single virus to a cantilever. However, this mass measurement is carried out in air after binding from solution and must assume that only a single object is bound to cantilever to estimate size; without *ex situ* high-resolution imaging this assumption may limit the utility of this sensitive technique. In addition, ion channels (21, 22) have the potential for electrically based single virus detection, although this has not been demonstrated to date for either single or multiplexed detection as we have shown.

The simplicity, single viral particle sensitivity, and capability of selective multiplexed detection of our approach suggest that this work could lead to useful viral sensing devices. Although parallel detection has been demonstrated for only two distinct viruses in this work, assembly methods have demonstrated much larger arrays of reproducible nanowire devices (14) that might simultaneously screen for the presence of 100 or more different viruses. Our use of antibodies to provide selectivity also has limitations common to immunoanalysis and PCR analysis methods (2) in the detection of rapidly mutating, engineered and/or new viruses. Yet, the potential to carry out multiplexing in large nanowire arrays could be exploited to overcome this limitation by including nanowires modified with general viral cell-surface

receptors (23) and antibody libraries. This could enable rapid identification of viral families and provide an indication of mutations in samples as required for robust medical and bioterrorism detection. Lastly, we believe these same capabilities and the potential to characterize a range of virus-receptor interactions could provide unique opportunities for fundamental virology and drug discovery.

We thank H. Park for discussion, S. Jin and K. Lin for help with the photolithography mask design, and B. Timko for help with electron microscopy. X.Z. thanks the Office of Naval Research and Searle Scholar program, and C.M.L. thanks the Defense Advanced Research Projects Agency, National Cancer Institute, and Ellison Medical Foundation for support of this work.

1. Strauss, E., Strauss, J. & Strauss, E. G. (2001) in *Viruses and Human Disease*, eds. Strauss, J. & Strauss, E. (Academic, San Diego), pp. 1–365.
2. Storch, G. A., ed. (1999) in *Essentials of Diagnostic Virology* (Churchill Livingstone, Edinburgh), pp. 1–25.
3. Stadler, K., Masignani, V., Eickmann, M., Becker, S., Abrignani, S., Klenk, H. D. & Rappuoli, R. (2003) *Nat. Rev. Microbiol.* **1**, 209–218.
4. Atlas, R. M. (2003) *Nat. Rev. Microbiol.* **1**, 70–74.
5. Niiler, E. (2002) *Nat. Biotechnol.* **20**, 21–25.
6. Elnifro, E. M., Ashshi, A. M., Cooper, R. J. & Klapper, P. E. (2000) *Clin. Microbiol. Rev.* **13**, 559–570.
7. Mackay, I. M., Arden, K. E. & Nitsche, A. (2002) *Nucleic Acids Res.* **30**, 1292–1305.
8. Cui, Y., Wei, Q., Park, H. & Lieber, C. M. (2001) *Science* **293**, 1289–1292.
9. Hahn, J. & Lieber, C. M. (2004) *Nano Lett.* **4**, 51–54.
10. Chen, R. J., Bangsaruntip, S., Drouvalakis, K. A., Kam, N. W. S., Shim, M., Li, Y. M., Kim, W., Utz, P. J. & Dai, H. J. (2003) *Proc. Natl. Acad. Sci. USA* **100**, 4984–4989.
11. Chen, R. J., Choi, H. C., Bangsaruntip, S., Yenilmez, E., Tang, X. W., Wang, Q., Chang, Y. L. & Dai, H. J. (2004) *J. Am. Chem. Soc.* **126**, 1563–1568.
12. Weiss, S. (2000) *Nat. Struct. Biol.* **7**, 724–729.
13. Zhuang, X. W. & Rief, M. (2003) *Curr. Opin. Struct. Biol.* **13**, 88–97.
14. Jin, S., Whang, D. M., McAlpine, M. C., Friedman, R. S., Wu, Y. & Lieber, C. M. (2004) *Nano Lett.* **4**, 915–919.
15. Lakadamyali, M., Rust, M. J., Babcock, H. P. & Zhuang, X. W. (2003) *Proc. Natl. Acad. Sci. USA* **100**, 9280–9285.
16. Cui, Y., Zhong, Z. H., Wang, D. L., Wang, W. U. & Lieber, C. M. (2003) *Nano Lett.* **3**, 149–152.
17. Steinfeld, J. I., Francisco, J. S. & Hase, W. L. (1998) in *Chemical Kinetics and Dynamics*, ed. Hart, M. (Prentice-Hall, Englewood Cliffs, NJ), pp. 124–132.
18. Herzer, S., Beckett, P., Wegman, T. & Moore, P. (2003) *Life Sci. News* **13**, 16–18.
19. Gardner, S. N., Kuczmariski, T. A., Vitalis, E. A. & Sleza, T. R. (2003) *J. Clin. Microbiol.* **41**, 2417–2427.
20. Gupta, A., Akin, D. & Bashir, R. (2004) *Appl. Phys. Lett.* **84**, 1976–1978.
21. Bayley, H. & Martin, C. R. (2000) *Chem. Rev.* **100**, 2575–2594.
22. Bayley, H. & Cremer, P. S. (2001) *Nature* **413**, 226–230.
23. Racaniello, V. R. (1996) *Proc. Natl. Acad. Sci. USA* **93**, 11378–11381.